Journal of Nuclear Medicine, published on February 9, 2017 as doi:10.2967/jnumed.116.185934

In vivo hypoxia PET imaging quantifies the severity of arthritic joint inflammation in line with overexpression of HIF and enhanced ROS generation

Kerstin Fuchs[1], Anna Kuehn[1], Moritz Mahling[1], Philipp Guenthoer[1], Andreas Hector[2], Dominik Hartl[2,3], Stefan Laufer[4], Ursula Kohlhofer[5], Leticia Quintanilla-Martinez[5], Gerald Reischl[1], Martin Röcken[6], Bernd J. Pichler[1], Manfred Kneilling[1,6]

1) Werner Siemens Imaging Center, Department of Preclinical Imaging and Radiopharmacy, Eberhard Karls University Tuebingen, 72076 Tuebingen, Germany

2) Children's Hospital of the Eberhard Karls University Tuebingen, 72076 Tuebingen, Germany

3.) Immunology, Inflammation and Infectious Diseases (I3) Discovery and Translational Area, Roche Pharma Research & Early Development (pRED), Roche Innovation Center Basel, 4070 Basel, Switzerland

4) Department of Pharmacy & Biochemistry, Eberhard Karls University Tuebingen, 72076 Tuebingen, Germany

5) Institute of Pathology and Neuropathology, Eberhard Karls University Tuebingen and Comprehensive Cancer Center, University Hospital Tuebingen, 72076 Tuebingen, Germany

6) Department of Dermatology, Eberhard Karls University Tuebingen, 72076 Tuebingen, Germany

Short title: *In vivo* hypoxia imaging in RA

Kerstin Fuchs, Werner Siemens Imaging Center, Department of Preclinical Imaging and Radiopharmacy, Eberhard Karls University Tuebingen, Roentgenweg 13, 72076 Tuebingen, Germany.

Email: kerstin.fuchs@med.uni-tuebingen.de

Phone: 07071-2983739, Fax: 07071-294451

Corresponding author: Manfred Kneilling, Werner Siemens Imaging Center, Department of Preclinical Imaging and Radiopharmacy and Department of Dermatology, Eberhard Karls University Tuebingen, Roentgenweg 13, 72076 Tuebingen, Germany.

Email: manfred.kneilling@med.uni-tuebingen.de; Phone: 07071-2986870

ABSTRACT

Hypoxia is essential for the development of autoimmune diseases such as rheumatoid arthritis (RA) and is associated with the expression of reactive oxygen species (ROS), due to enhanced infiltration of immune cells. The aim of this study was to demonstrate the feasibility of measuring hypoxia non-invasively *in vivo* in arthritic ankles with positron emission tomography (PET)/magnetic resonance imaging (MRI) using the hypoxia tracers ^{18}F-fluoromisonidazole (FMISO) and ^{18}F-fluoroazomycinarabinoside (FAZA). Additionally, we quantified temporal dynamics of hypoxia and ROS stress using L-012, a ROS-sensitive chemiluminescence optical imaging (OI) probe, and analyzed the activation of hypoxia inducible factors (HIFs). **Methods:** Mice underwent non-invasive *in vivo* PET/MRI to measure hypoxia or OI to analyze ROS expression. Additionally, we performed *ex vivo* pimonidazole-/HIF-1α-immunohistochemistry and HIF-1α/2α-western blot/mRNA-analysis of inflamed and healthy ankles to confirm our *in vivo* results. **Results:** Mice diseased from experimental RA exhibited a 3-fold enhancement in hypoxia tracer uptake, even in the very early disease stages, and a 45-fold elevation in ROS-expression in inflamed ankles compared with the ankles of healthy controls. We further found strong correlations of our non-invasive *in vivo* hypoxia PET data with pimonidazole and expression of HIF-1α in arthritic ankles. The strongest hypoxia tracer uptake was observed as soon as day 3, whereas the most pronounced ROS stress was evident on day 6 after the onset of experimental RA, indicating that tissue hypoxia can precede ROS stress in RA. **Conclusion:** Collectively, for the first time, we have demonstrated that non-invasive measurement of hypoxia in inflammation using ^{18}F-FAZA/^{18}F-FMISO-PET imaging represent a promising new tool for uncovering and monitoring rheumatic inflammation *in vivo*. Further, as hypoxic inflamed tissues are associated with overexpression of HIFs, specific inhibition of HIFs might represent a new powerful treatment strategy.

Keywords: Rheumatoid Arthritis, i*n vivo* hypoxia imaging, PET, HIF, ROS

INTRODUCTION

RA is one of the most common autoimmune diseases with a prevalence of 0.5-1 % in the Western world population (*1*). RA is a common cause of permanent disability and is characterized by chronic inflammation of the synovial tissues associated with a dense leukocytic infiltrate, angiogenesis, pannus formation and ultimately cartilage and bone destruction (*2*).

We recently demonstrated that ^{18}F-galacto-RGD PET-imaging is applicable to the early detection of angiogenesis in experimental glucose-6-phosphate-isomerase (GPI)-induced arthritis (*3*). Interestingly, enhanced αvβ3-integrin activity in the synovial vasculature of arthritic joints is associated with the onset of hypoxia (*4*).

In addition, hypoxia induces the formation of the transcription factors HIFs, which trigger an up-regulation of pro-angiogenic factors and mediators involved in glycolysis (*4*). The HIF pathway allows cells to survive during hypoxic conditions and plays a major role in RA disease progression, whereas especially HIF-1α acts as a key regulator of inflammation (*5*). Cramer *et al.* reinforced the essential role of hypoxia and HIF-1α expression in GPI-induced arthritis in HIF-1α$^{-/-}$ mice that exhibited reduced joint inflammation, whereas wild-type mice developed severe joint inflammation (*6*).

Therapeutic approaches targeting HIF associated pathways are developed mainly in cancer research, including HIF-inhibitors, hypoxic prodrugs or specific antibodies (*7*). Different treatment strategies targeting HIF or downstream mechanisms such as vascular endothelial growth factor, demonstrated promising results in small animals, but need to be further evaluated in clinical trials (*5*). Additionally, hypoxia is frequently associated with the expression of ROS, which are additional key players in angiogenesis (*4*). In contrast to hypoxia, the roles of ROS and ROS-scavengers in arthritic joint inflammation remain ambiguous because different studies have reported either pro- or anti-inflammatory effects of different ROS components and ROS-scavengers (*8*).

To date, the clinically applied state of the art imaging modalities for the diagnosis of RA in patients are MRI and power Doppler ultrasonography. Non-invasive imaging of inflammation-induced hypoxia in arthritic joint-inflammation with a PET/MRI system and a hypoxia-specific radiotracer might be an additional promising clinical tool for uncovering clinically silent joints at a very early stage. This early discovery is of particular importance because the early treatment of RA patients in the so-called “window of opportunity” is essential to achieving complete remission. Additionally, longitudinal monitoring and the demonstration of complete RA-remission via PET/MRI might allow one to minimize the duration of immunosuppressive treatment, especially in children.

Currently, ^{18}F-FMISO is among the commonly clinically applied nitroimidazole-based hypoxia tracer that facilitates the identification of tumor hypoxia in patients with malignancies (*9*) followed by ^{18}F- FAZA (*10*). Both nitroimidazole-based radiolabeled tracers are trapped exclusively in hypoxic cells (*11*). ROS stress can be monitored non-invasively *in vivo* with L-012, which is a chemiluminescence reporter OI probe that predominantly reacts with hydroxyl radicals and hypochlorous acid (*12*) and is able to indicate ROS/reactive nitrogen species (RNS) release during inflammation (*13*).

The aim of this study was to investigate the potential of non-invasive *in vivo* ^{18}F-FMISO/^{18}F-FAZA-PET and MRI for the quantification of hypoxia in the inflamed joints of mice with experimental GPI-induced arthritis. We correlated our *in vivo* ^{18}F-FMISO/^{18}F-FAZA-PET/MRI data with HIF-1α- and HIF-2α-protein expressions and immunohistological pimonidazole staining. Additionally, we aimed to uncover a potential cross-correlation between hypoxia and ROS-stress in RA.

MATERIALS AND METHODS

GPI-Induced Arthritis

GPI-arthritis was induced as described (*14*) (Suppl. Material and Methods). The animal studies were approved by the Regierungspraesidium Tuebingen and conducted according to approved animal use and care protocols of the German Animal Protection Law.

In vivo PET Imaging

In vivo high-resolution PET-images were acquired with a small animal Inveon microPET scanner (Siemens Medical Solutions USA, Inc., Knoxville, TN, USA) as described in Fuchs *et al.* (*14*). The kinetic data acquired for 90-min after tracer injection and static scans were acquired after an uptake time of 60-min and a conscious tracer uptake. ^{18}F-FAZA and ^{18}F-FMISO were injected *i.v.* and PET-acquisitions were performed on days 1, 3 and 6 after one GPI-/control-serum transfer.

Determination of ROS-Stress by OI

We measured ROS-expression on days 3 and 6 after one GPI-/control-serum transfer using L-012 (5 mg/mL), which is a luminescent probe that was purchased from Wako Chemical (Neuss, Germany). L-012 was

dissolved in ultrapure H_2O and administered *i.v.*, with an injection volume of 100 µL. For *in vivo* investigations, we used the IVIS Spectrum OI System (Perkin Elmer, Rodgau-Jügesheim, Germany). OI measurements were performed immediately after the injection of L-012. The mice were anesthetized via the inhalation of isoflurane-O_2 (Abbott GmbH) and warmed to maintain body temperature at 37 °C. Regions of interest were drawn on the right and left ankles to enable a semi-quantitative-analysis of the average radiance [p/s/cm^2/sr] of the chemiluminescence. The image analyses were performed with Living Image Software (Perkin Elmer).

Invasive pO_2-Probe Measurements

At day 6 after arthritic induction, we placed calibrated pO_2-probes (BF/OFT/E; bore ~ 450 µm, Oxford Optronix Ltd., Oxford, U.K.) in the centers of the ankle joint spaces of the arthritic- and healthy-mice (1.5 % isoflurane anesthesia) and the contralateral *gastrocnemius muscle* as a control. The pO_2-data were recorded using PowerLab (PowerLab 16/35, AD Instruments GmbH) and analyzed with LabChart (LabChart 7.2, AD Instruments GmbH).

Fluorescence-activated cell sorting, Radiopharmaceutical, Autoradiography, Simultaneous PET/MRI, Histological Analysis, Western Blot Analysis, Real-time Polymerase Chain Reaction and Statistical Data Analysis

Please refer to the Supplemental Material & Methods for more detailed information.

RESULTS

Invasive *in vivo* pO_2-Measurements in the Arthritic Ankles

To analyze the low pO_2-values in the arthritic ankles, we performed *in vivo* pO_2-measurements using an invasive pO_2-probe at 6 days after onset of arthritis. As expected, we observed significantly reduced pO_2-values in the arthritic ankles (16.9 mmHg (8.0 – 24.9 mmHg), median (25% - 75% quartile)) compared with the healthy control ankles (36.8 mmHg (30.3 – 40.8 mmHg), p=0.02, Mann–Whitney U test, (Fig. 1A, left plot). In contrast, the pO_2-values in the muscle tissues displayed no differences between the GPI-arthritic (71.0 mmHg (51.6 – 72.4 mmHg)) and healthy (63.1 mmHg (56.2 – 71.6 mmHg)) mice (Fig. 1A, right plot). We correlated ankle swelling [mm] with the pO_2-values from the arthritic- and healthy-ankles and observed a superior Pearson product-moment

correlation coefficient (PPMCC, r=-0.86, Fig. 1B). All animals used for this experiment demonstrated similar ankle swellings (Supplemental Fig. 1A).

Quantitative non-invasive *in vivo* ^{18}F-FMISO/^{18}F-FAZA-PET-Imaging of Hypoxia in Inflamed Ankles

First, we injected ^{18}F-FMISO into mice with severe ankle-inflammation 6 days after GPI- or control-serum transfer and conducted *in vivo* PET-investigations. Representative ^{18}F-FMISO-PET-images of an arthritic- and a control-mouse are presented in Figure 2A (left column) and demonstrate a strongly enhanced ^{18}F-FMISO-uptake in the arthritic-, compared with the healthy-ankles. The time-activity-curves (TAC), which were corrected for the ^{18}F half-life and the injected dose, of the 90-min dynamic PET-scans focusing on the ankles of the arthritic- and healthy-mice revealed an early injection peak in the arthritic-ankles followed by a slight decrease and steady-state tracer-accumulation at 30-min. These findings indicated intense hypoxic areas in the inflamed-joints. The TACs of the healthy ankles (control mice) exhibited a slight injection peak followed by steady-state tracer-accumulation **(**Fig. 2A, central column). Quantitative analysis of the 10-min static ^{18}F-FMISO (Fig. 2C, right column; 30-min after ^{18}F-FMISO-injection**)** revealed a 2.7-fold enhancement of ^{18}F-FMISO in the inflamed-, compared with the healthy-ankles (arthritic: 3.0±0.5 % ID/cm^3; healthy: 1.1±0.2 % ID/cm^3; $p< 0.001$).

To strengthen our ^{18}F-FMISO data, we injected the second hypoxia tracer, i.e., ^{18}F-FAZA, into arthritic-, and healthy-mice (Fig. 2B, left column**)**. Similar to the ^{18}F-FMISO results, we observed an enhanced ^{18}F-FAZA-uptake in the inflamed-, compared with the healthy-ankles. The 90-min ^{18}F-FAZA-TACs were similar to the ^{18}F-FMISO-TACs and revealed an early injection-peak in the arthritic-ankles followed by a quite strong decrease and steady-state tracer-accumulation at 60-min. The TAC of the ankles of the healthy mice lacked the injection peak and reached a plateau after 40-min **(**Fig. 2B, central column**)**. Quantitative analysis of the 10-min static ^{18}F-FAZA-scans (Fig. 2B, right column; 60-min after ^{18}F-FAZA-injection**)** revealed a 2.8-fold enhancement of ^{18}F-FAZA-uptake in the inflamed-, compared with the healthy-ankles (arthritic: 1.4±0.5 % ID/cm^3; healthy: 0.5±0.28 % ID/cm^3; $p< 0.001$).

Next, we focused on the feasibility of the use of hypoxia-tracers to detect the early stages of experimental arthritis. To this end, we injected ^{18}F-FMISO into littermates on days 1, 3 and 6 after GPI- or control-serum injection and performed static PET-scans that focused on the ankles. 24-hours after the onset of GPI-arthritis, we observed no enhancement of hypoxia tracer uptake (arthritic: 1.4±0.2 % ID/cm^3; healthy: 1.3±0.1 % ID/cm^3), whereas on day

three, a significantly enhanced ^{18}F-FMISO uptake was observed in the arthritic-ankles (arthritic: 3.3±0.4 % ID/cm^3; healthy: 1.5±0.1 % ID/cm^3; p= 0.002). On day 6, quantitative analysis of the 10-min static ^{18}F-FMISO-PET scans (30-min after ^{18}F-FMISO-injection) indicated a 2.7-fold enhancement in ^{18}F-FMISO-uptake in the inflamed-, compared with the healthy-ankles (arthritic: 3.0±0.5 % ID/cm^3; healthy: 1.1±0.2 % ID/cm^3; p< 0.001, Fig. 2C, left). Additionally, we correlated the ^{18}F-FMISO-uptake (% ID/ cm^3) with ankle swelling [mm] on all investigated days and observed good correlations between the ^{18}F-FMISO-uptake and ankle swelling (the PPMCC was r=0.88, Fig. 2C, right). All animals used for these experiments demonstrated similar ankle swellings (Supplemental Figs. 1B-1D, Supplemental Figs. 2 A and 2B).

Simultaneous non-invasive *in vivo* PET/MRI Measurements

High-resolution simultaneous PET/MRI investigations provided temporal and spatial information about the hypoxia tracer-uptake in the inflamed-, and healthy-ankles. MRI yielded detailed anatomical information with high soft-tissue contrast. The simultaneous ^{18}F-FMISO-PET/MR-images indicated that the severe ankle swelling and pronounced accumulation of synovial fluid within the joint spaces of the arthritic ankles correlated well with the sites of ^{18}F-FMISO-uptake. The MRI-investigations of the ankles of healthy mice appeared normal (Fig. 3).

***Ex vivo* Autoradiography-Analysis and Pimonidazole Staining confirmed the ^{18}F-FMISO/^{18}F-FAZA-PET Data**

We sacrificed the mice immediately after the *in vivo* PET-investigations, sliced the ankles (20 µm), and placed them on a phosphor screen for *ex vivo* autoradiography-analysis. The inflamed ankles exhibited enhanced ^{18}F-FMISO/^{18}F-FAZA-uptake with hot spots, (Fig. 4A) similar to the findings of the PET-examinations (Figs. 2 and 3), whereas only a low and almost uniform ^{18}F-FMISO/^{18}F-FAZA-uptake was observed in the control-ankles. Because pimonidazole accumulates within hypoxic regions via a basic mechanism that is identical to that of the hypoxia tracer ^{18}F-FMISO/^{18}F-FAZA, we conducted pimonidazole-immunohistochemistry of the arthritic-(Fig. 4B, right images) and healthy-ankles (Fig. 4B, left images) 6 days after one GPI- or control-serum injection. Clearly distinct visible dense areas (i.e., hot spots similar to our PET-, and autoradiography-data) of accumulated inflammatory cells in the synovia stained positive for pimonidazole. No inflammatory cells were found in the ankles of the healthy-mice, and none of the resident cells (with the exception of presumably specific staining of sebaceous glands (*15*)) stained positive for pimonidazole.

HIF-1α Immunohistochemistry and HIF-1/HIF-2α Western Blot (WB) and rtPCR Analyses support the onset of Hypoxia

Next, we conducted hematoxylin & eosin staining and HIF-1α immunohistochemistry of the arthritic-, (Fig. 5A; upper right and lower right image) and healthy-ankles (Fig. 5A; upper left and lower left). At day 6 after GPI-serum transfer inflamed ankles revealed high number of infiltrating inflammatory cells composed of neutrophils, mononuclear cells and fibroblasts. In some cases, early phases of bone destruction were observed, and the synovial membrane covered the articular surface of the joint. Fibrosis and focally thinned and wasted articular cartilage were observed. The ankles of the healthy control mice exhibited normal joint structures with no signs of inflammation. HIF-1α-immunohistological staining of arthritic-ankles revealed a high number of local and infiltrated cells with positive HIF-1α staining mainly composed of neutrophils and synoviocytes (Fig. 5A, lower right image). HIF-1α-staining of the healthy-ankles revealed negative results (Fig. 5A, lower left image).

For a quantitative analysis of the HIF-1α-, and HIF-2α-expression in the inflamed-, and healthy-ankles, we performed WB analysis. The inflamed arthritic-ankles displayed strong HIF-1α and HIF-2α protein-expressions (at day 6 after one GPI-serum injection) in the nuclear fraction (n) and strong but lower expressions in the cytosolic fraction (c); only a slight HIF-1α/2α protein-expressions was determined in healthy ankles (Fig. 5B).

RT-PCR analyses of the expression levels of HIF-1α and HIF-2α mRNA in the inflamed-ankles revealed no increase in HIF-1α mRNA-expression after the first GPI-serum injection, but strong 28-fold up-regulation 6-hours after a second GPI-serum injection (48-hours after the first GPI-serum injection). HIF-2α mRNA-expression increased 6-fold, 6-hours after the first, and 9-fold, 6-hours after the second GPI-serum injection (Fig. 5C, upper bars). Focusing on the pro-inflammatory cytokines, we found a 9-fold enhancement of IL1β mRNA-expression 6-hours after the first GPI-serum injection and a 68-fold and 7-fold increase in IL1β mRNA and TNF mRNA-expression, respectively, 6-hours after the second GPI-serum injection (Fig. 5C, lower bars).

Hypoxia is associated with ROS Stress

To corroborate our ROS stress hypothesis, we evaluated the onset of ROS stress non-invasively *in vivo* with OI using L-012, at day 3 and 6 after one GPI-/control-serum injection. Our investigations revealed impressive L-012-derived signal intensity (SI) in the ankles and paws of the arthritic mice, but no signal was noted in the joints of the

healthy mice (Fig. 6A). Quantitative analysis of the L-012 SI, yielded a 57-fold, statistically significant ($p<0.0001$) enhancement of the average radiance SI [p/s/cm²/sr] in the arthritic ankles on day 6 (165639 [p/s/cm²/sr]) compared with the healthy ankles (2904 [p/s/cm²/sr]). On day 3 (80544 [p/s/cm²/sr]), we observed a 28-fold significant ($p<0.0001$) enhancement of the SI of L-012 compared with the control-ankles (Fig. 6A). All animals used for this experiment demonstrated similar ankle swellings (Supplemental Fig. 2C). Furthermore, we correlated the L-012 SI [p/s/cm²/sr] with ankle swelling [mm] on all investigated days (control and arthritis on days 3 and 6) and found a good PPMC of $r=0.72$ (Fig. 6B).

Additionally, we isolated the cellular infiltrates from ankle joint lavages of the arthritic-, and healthy-mice (at day 6) and performed FACS-analysis using dihydrorhodamine (DHR) staining, which is used to identify ROS-intermediate expressing leukocytes. The DHR-FACS analysis revealed a 45-fold enhancement of the expression of reactive oxygen intermediates (geometric mean of DHR positive cells) in the joint lavages of the arthritic ankles (214.3) compared with the lavages of the healthy ankles (4.7) (Fig. 6C). Thus, our non-invasive *in vivo* L-012 OI measurements and *ex vivo* DHR-FACS analysis clearly demonstrated a strong correlation between hypoxia and ROS-stress in the inflamed ankles.

DISCUSSION

In this study, we experimentally verified that ^{18}F-FMISO-/^{18}F-FAZA-PET imaging is feasible for uncovering inflammation-induced hypoxia non-invasively *in vivo* in arthritic joints. We confirmed the presence of tissue hypoxia in the inflamed ankles *in vivo* with an invasive pO_2-probe and found significantly reduced interstitial pO_2-values in the articular ankle joint-spaces of the arthritic mice compared with the healthy mice (Fig. 1). In 2004, Baudelet and Gallez *et al.* used an identical invasive system to investigate the influences of different anesthetics on interstitial pO_2 values in tumors (*16*). The activation of infiltrating and resident cells is associated with strongly enhanced glucose metabolism and O_2 consumption and is thus likely responsible for hypoxia and hypoxia-induced angiogenesis (*17*).

As early as 1979, Chapman *et al.* recommended radioactively labeled 2-nitroimidazoles, such as ^{18}F-FMISO, for non-invasive *in vivo* PET-imaging of hypoxia (*18*). Local oxygen tension is the major parameter that causes ^{18}F-FMISO-retention in cells by ligation to intracellular macromolecules. ^{18}F-FMISO-retention is dependent on the activity of nitroreductase, which leads to the reduction of an NO_2 group and the formation of an imidazole ring (*19*). Currently, ^{18}F-FMISO is the best-characterized and established hypoxia tracer and is commonly used in clinical and preclinical cancer studies to monitor anti-cancer therapies (*20*).

Our ^{18}F-FMISO-PET studies revealed significantly enhanced hypoxia tracer-uptake in the arthritic ankles compared with the control ankles on day 6 (Fig. 2C), which verifies ^{18}F-FMISO as an applicable marker for the detection of early RA because ^{18}F-FMISO-PET uptake correlated well with the observed ankle swelling in these experiments. ^{18}F-FAZA is a second hypoxia tracer with favorable pharmacokinetics and tracer clearance. We obtained similar results with this tracer, which strengthens our data regarding hypoxia and PET-imaging of inflammation-induced hypoxia in arthritic ankles (Fig. 2) (*10,11,21*).

Our hypoxia-PET studies further uncovered an enhanced ^{18}F-FMISO-uptake in the inflamed and healthy ankles as well as a clearly visible enhanced whole-body tracer uptake ratio compared with ^{18}F-FAZA. However, most importantly, the arthritic-, and healthy-ankles produced similar results with both hypoxia tracers (ratio ^{18}F-FMISO: 2.7; ratio ^{18}F-FAZA: 2.8). This phenomenon can be explained by the faster ^{18}F-FAZA tissue clearance, which resulted in a reduced ^{18}F-FAZA background. Another reason for the differences in the ^{18}F-FMISO and ^{18}F-FAZA tracer distributions could be the greater hydrophilicity of ^{18}F-FAZA compared with ^{18}F-FMISO (*21*).

We used simultaneous ^{18}F-FMISO/^{18}F-FAZA-PET/MRI to identify the exact anatomical sites (bone and soft tissue) of hypoxia in the inflamed ankles/joints (Fig. 3). MRI additionally enables the identification of inflammation-induced changes in soft tissues, such as edema, thickening of the synovia and pannus formation. (*14*). ^{18}F-FMISO-PET/MRI focused on the inflamed ankles indicated severe ankle swelling and a pronounced accumulation of synovial fluid within the joint spaces of the arthritic ankles that correlated well with the sites of ^{18}F-FMISO-uptake (Fig. 3).

Several *ex vivo* methods are available to identify sites of hypoxia in tissues, for example, the detection of *i.v.* administered nitroimidazoles, such as pimonidazole, depicts hypoxic-regions (*22*) as do analyses of regulatory proteins and genes (HIF-1α and HIF-2α protein/mRNA) after biopsy. Thus, using pimonidazole, which is a bioreactive chemical substance that accumulates in regions with low pO_2-values and forms protein-adducts in living hypoxic cells (*23*), we were able to confirm our *in vivo* ^{18}F-FMISO/^{18}F-FAZA-PET results (Fig. 4B). Furthermore, to validate our hypoxia-PET results on the molecular level, we performed WB-analyses of lysates derived from the arthritic-, and healthy-ankles In this context, it is important to mention that approximately 1-5 % of all human genes are regulated in response to hypoxia, mainly through HIF (*24*). An oxygen content of <5-10 % causes the accumulation and activation of HIF-1α, which induces angiogenesis-promoting growth factors (*25*). The role of HIF-1 in cancer biology is well accepted, and thus far several studies have proven that HIFs coordinate different levels of immune responses (*26*). During inflammation, hypoxia is caused by a massive infiltration and activation of neutrophils and mononuclear leukocytes and by activated proliferating resident cells (macrophages, synovial/endothelial cells). This processes results in enhanced expression of the transcription factors HIF-1α and HIF-2α (*27*). The transcription factor HIF-1α is constitutively expressed and stabilized during hypoxia, which leads to increased expression levels of pro-angiogenic mediators.

Several previous studies have confirmed that mitochondria-generated ROS under low-oxygen conditions are responsible for the activation of HIF during hypoxia (*28,29*). Additionally, HIF-1α is primarily responsible for the acute hypoxic-response and prolongs the survival of neutrophils via the inhibition of apoptosis (*30*). Cramer *et al.* uncovered the superior importance of HIF-1α in GPI-arthritis. Thus, hypoxia-driven HIF-1α expression appears to be essential in experimental arthritis (*6*). In line with these data, Westra *et al.* demonstrated that sustained HIF-2α-expression is important for RA development (*31*). Similar results were observed by Ryu *et al* in 2014, demonstrating

that activation of HIF-2α is needed to induce RA, as HIF-2α-deficient mice revealed reduced arthritic joint inflammation (*32*) (Inflammation and ROS: supplemental discussion).

Kielland *et al.* demonstrated that L-012 is a useful probe for *in vivo* determination of ROS/RNS-stress in different inflammation models. Thus, L-012 is a functional OI probe that emits light from sites of ROS/RNS-release in a spatial and temporal manner (*13*). Imada *et al.* demonstrated that the L-012 signal is strongly induced by stimulated neutrophils (*33*), which verifies L-012 as a tool for measuring ROS/RNS during inflammatory processes. Hence, we used the L-012 probe to demonstrate ROS/RNS-stress in arthritic joints. At the time-point with the most severe ankle swelling, i.e., day 6 after the onset of arthritis, we observed the most pronounced ROS-stress (Fig. 6B), which clearly indicated that strong hypoxia in arthritic-joint disease is evident even before the appearance of strong ROS-stress.

Several research groups claim that ROS are mainly produced during acute hypoxia. Thus, the inhibition of ROS-stress at the early onset of disease could protect against chronic-hypoxia and the establishment of the chronic-inflammation that is responsible for tissue damage (*34*). Because the development of inflammation due to hypoxia is clinically important (*35*), non-invasive *in vivo* PET-imaging of inflammation-induced hypoxia during the initial phases of RA might enable the identification of early pathological changes even before the onset of cartilage and joint-destruction. Thus, we demonstrated for the first time that hypoxia PET-imaging using ^{18}F-FMISO or ^{18}F-FAZA is applicable for the visualization and monitoring of RA ankles. Moreover, we uncovered a different temporal dynamic of hypoxia and ROS-stress and found that hypoxia accrues with enhanced ROS-stress.

CONCLUSION

Non-invasive *in vivo* hypoxia-PET imaging represents an important new tool for identifying the early stages of inflammation and monitoring therapeutic interventions in the clinic for patients with RA. The *in vivo* specification of the different temporal dynamics of hypoxia (associated with expression of HIFs) and ROS/RNS-expression could be of paramount importance in terms of an individualized therapeutic approach for RA-patients, especially as specific inhibition of HIFs might represent a new promising treatment approach.

ACKNOWLEDGMENTS

We thank Daniel Bukala, Funda Cay and Walter Ehrlichmann, Werner Siemens Imaging Center, Laboratory for Preclinical Imaging and Radiopharmacy, University of Tuebingen, for their excellent technical support of the study.

Financial Support: Supported by Werner Siemens Imaging Center, Department of Preclinical Imaging and Radiopharmacy, Eberhard Karls University Tuebingen and by the DFG through the CRC 156 (project C03).

REFERENCES

1. Feldmann M, Brennan FM, Maini RN. Rheumatoid arthritis. *Cell.* 1996;85:307-310.

2. Firestein GS. Immunologic mechanisms in the pathogenesis of rheumatoid arthritis. *J Clin Rheumatol.* 2005;11:S39-44.

3. Kneilling M, Hultner L, Pichler BJ, et al. Targeted mast cell silencing protects against joint destruction and angiogenesis in experimental arthritis in mice. *Arthritis Rheum.* 2007;56:1806-1816.

4. Taylor PC, Sivakumar B. Hypoxia and angiogenesis in rheumatoid arthritis. *Curr Opin Rheumatol.* 2005;17:293-298.

5. Hua S, Dias TH. Hypoxia-Inducible Factor (HIF) as a target for novel therapies in rheumatoid arthritis. *Front Pharmacol.* 2016;7:184.

6. Cramer T, Yamanishi Y, Clausen BE, et al. HIF-1alpha is essential for myeloid cell-mediated inflammation. *Cell.* 2003;112:645-657.

7. Wigerup C, Pahlman S, Bexell D. Therapeutic targeting of hypoxia and hypoxia-inducible factors in cancer. *Pharmacol Ther.* 2016;164:152-169.

8. Poteet E, Winters A, Yan LJ, et al. Neuroprotective actions of methylene blue and its derivatives. *PLoS One.* 2012;7:e48279.

9. Piert M, Machulla H, Becker G, et al. Introducing fluorine-18 fluoromisonidazole positron emission tomography for the localisation and quantification of pig liver hypoxia. *Eur J Nucl Med.* 1999;26:95-109.

10. Piert M, Machulla HJ, Picchio M, et al. Hypoxia-specific tumor imaging with 18F-fluoroazomycin arabinoside. *J Nucl Med.* 2005;46:106-113.

11. Piert M, Machulla HJ, Becker G, Aldinger P, Winter E, Bares R. Dependency of the [18F]fluoromisonidazole uptake on oxygen delivery and tissue oxygenation in the porcine liver. *Nucl Med Biol.* 2000;27:693-700.

12. Wen Y, Li W, Poteet EC, et al. Alternative mitochondrial electron transfer as a novel strategy for neuroprotection. *J Biol Chem.* 2011;286:16504-16515.

13. Kielland A, Blom T, Nandakumar KS, Holmdahl R, Blomhoff R, Carlsen H. In vivo imaging of reactive oxygen and nitrogen species in inflammation using the luminescent probe L-012. *Free Radic Biol Med.* 2009;47:760-766.

14. Fuchs K, Kohlhofer U, Quintanilla-Martinez L, et al. In vivo imaging of cell proliferation enables the detection of the extent of experimental rheumatoid arthritis by 3'-deoxy-3'-18f-fluorothymidine and small-animal PET. *J Nucl Med.* 2013;54:151-158.

15. Cobb LM, Nolan J, Butler SA. Distribution of pimonidazole and RSU 1069 in tumour and normal tissues. *Br J Cancer.* 1990;62:915-918.

16. Baudelet C, Gallez B. Effect of anesthesia on the signal intensity in tumors using BOLD-MRI: comparison with flow measurements by Laser Doppler flowmetry and oxygen measurements by luminescence-based probes. *Magn Reson Imaging.* 2004;22:905-912.

17. Semenza GL. Hypoxia-inducible factor 1: control of oxygen homeostasis in health and disease. *Pediatr Res.* 2001;49:614-617.

18. Chapman JD. Hypoxic sensitizers--implications for radiation therapy. *N Engl J Med.* 1979;301:1429-1432.

19. Padhani AR, Krohn KA, Lewis JS, Alber M. Imaging oxygenation of human tumours. *Eur Radiol.* 2007;17:861-872.

20. Hendrickson K, Phillips M, Smith W, Peterson L, Krohn K, Rajendran J. Hypoxia imaging with [F-18] FMISO-PET in head and neck cancer: potential for guiding intensity modulated radiation therapy in overcoming hypoxia-induced treatment resistance. *Radiother Oncol.* 2011;101:369-375.

21. Reischl G, Dorow DS, Cullinane C, et al. Imaging of tumor hypoxia with [124I]IAZA in comparison with [18F]FMISO and [18F]FAZA--first small animal PET results. *J Pharm Pharm Sci.* 2007;10:203-211.

22. Sorensen BS, Horsman MR, Vorum H, Honore B, Overgaard J, Alsner J. Proteins upregulated by mild and severe hypoxia in squamous cell carcinomas in vitro identified by proteomics. *Radiother Oncol.* 2009;92:443-449.

23. Rademakers SE, Lok J, van der Kogel AJ, Bussink J, Kaanders JH. Metabolic markers in relation to hypoxia; staining patterns and colocalization of pimonidazole, HIF-1alpha, CAIX, LDH-5, GLUT-1, MCT1 and MCT4. *BMC Cancer.* 2011;11:167.

24. Semenza GL. Targeting HIF-1 for cancer therapy. *Nat Rev Cancer.* 2003;3:721-732.

25. Dayan F, Mazure NM, Brahimi-Horn MC, Pouyssegur J. A dialogue between the hypoxia-inducible factor and the tumor microenvironment. *Cancer Microenviron.* 2008;1:53-68.

26. Nizet V, Johnson RS. Interdependence of hypoxic and innate immune responses. *Nat Rev Immunol.* 2009;9:609-617.

27. Ema M, Taya S, Yokotani N, Sogawa K, Matsuda Y, Fujii-Kuriyama Y. A novel bHLH-PAS factor with close sequence similarity to hypoxia-inducible factor 1alpha regulates the VEGF expression and is potentially involved in lung and vascular development. *Proc Natl Acad Sci U S A.* 1997;94:4273-4278.

28. Kaelin WG, Jr. ROS: really involved in oxygen sensing. *Cell Metab.* 2005;1:357-358.

29. Brunelle JK, Bell EL, Quesada NM, et al. Oxygen sensing requires mitochondrial ROS but not oxidative phosphorylation. *Cell Metab.* 2005;1:409-414.

30. Walmsley SR, Print C, Farahi N, et al. Hypoxia-induced neutrophil survival is mediated by HIF-1alpha-dependent NF-kappaB activity. *J Exp Med.* 2005;201:105-115.

31. Westra J, Molema G, Kallenberg CG. Hypoxia-inducible factor-1 as regulator of angiogenesis in rheumatoid arthritis - therapeutic implications. *Curr Med Chem.* 2010;17:254-263.

32. Ryu JH, Chae CS, Kwak JS, et al. Hypoxia-inducible factor-2alpha is an essential catabolic regulator of inflammatory rheumatoid arthritis. *PLoS Biol.* 2014;12:e1001881.

33. Imada I, Sato EF, Miyamoto M, et al. Analysis of reactive oxygen species generated by neutrophils using a chemiluminescence probe L-012. *Anal Biochem.* 1999;271:53-58.

34. Hodyc D, Johnson E, Skoumalova A, et al. Reactive oxygen species production in the early and later stage of chronic ventilatory hypoxia. *Physiol Res.* 2012;61:145-151.

35. Eltzschig HK, Carmeliet P. Hypoxia and inflammation. *N Engl J Med.* 2011;364:656-665.

Figure 1

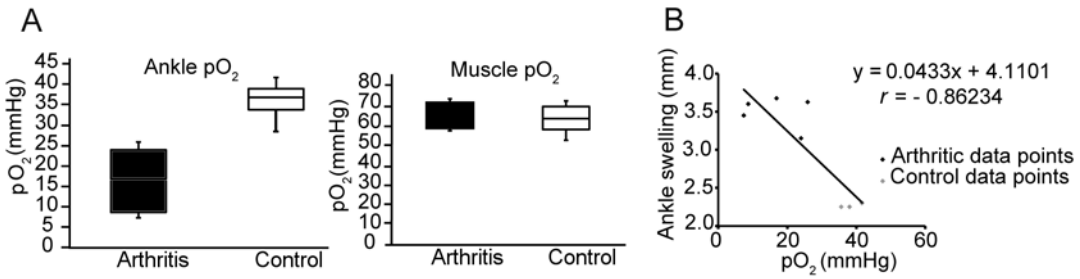

(A) pO_2-values in arthritic- (gray) and healthy-ankles (white) (left box plot) and the contralateral muscle-tissues (right box plot) on day 6 after GPI- (n=5) or control-serum (n=4) injection. (B) We correlated ankle-swelling (mm) and the pO_2-values from the arthritic-, and healthy-ankles.

Figure 2

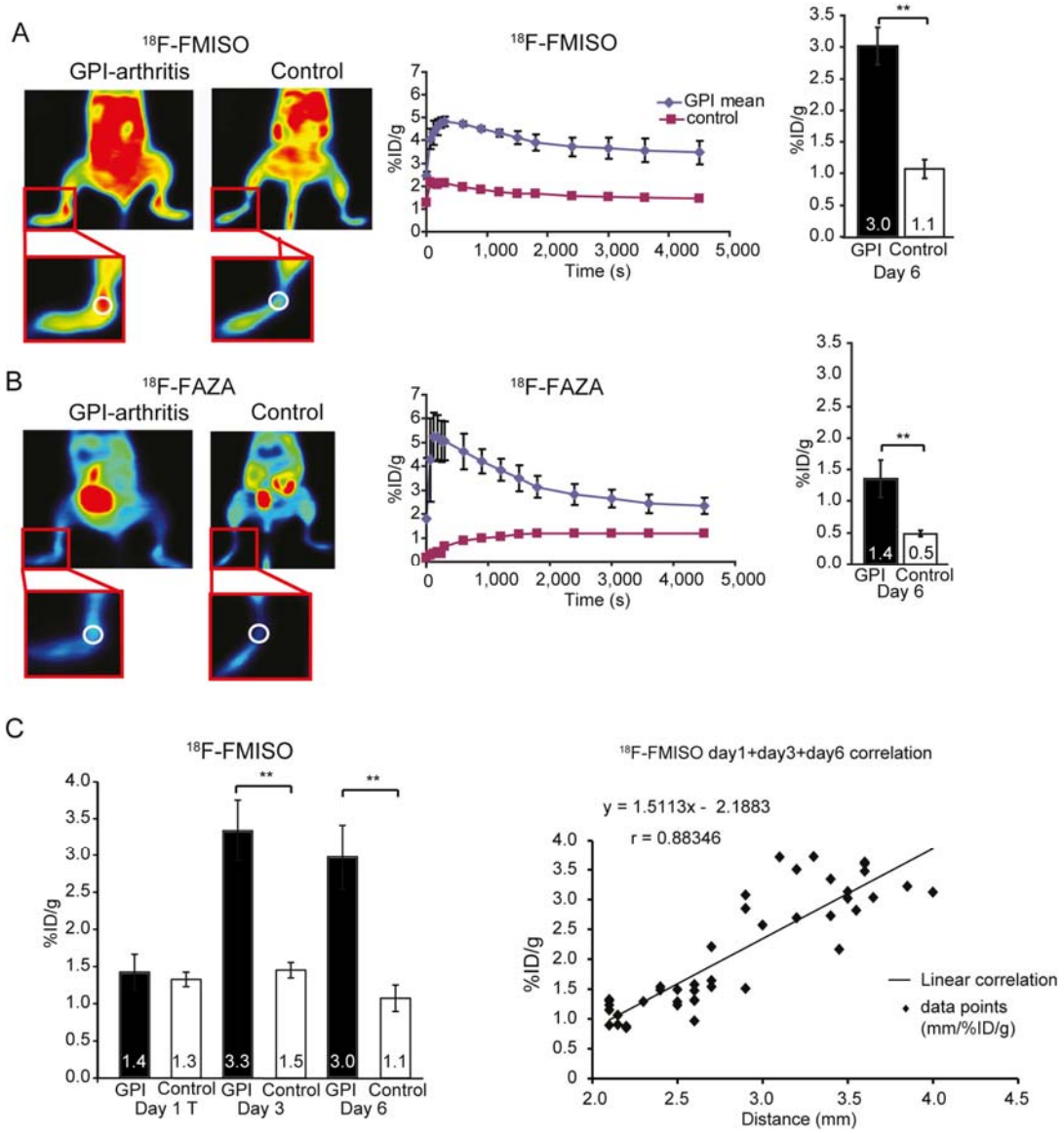

(A) Representative ^{18}F-FMISO-, (first column) and (B) ^{18}F-FAZA-PET (first column) images from arthritic,- and healthy-control mice on day 6 after GPI- or control-serum injection (single slices of 90-min data sets). 90-min ^{18}F-FMISO- (GPI n=2, control n=1) (A, second column) and ^{18}F-FAZA-TACs (GPI n=2, control n=1) (B, second column) on day 6 after GPI- or control-serum application. Quantification of the pooled static ^{18}F-FMISO-, (GPI n=8, control n=5) (A, third column) and ^{18}F-FAZA-PET (GPI n=8, control n=4) (B, third column) of arthritic-, and healthy-ankles presented as the means of the % ID/g ± SDs. (C) Quantification of the pooled static ^{18}F-FMISO-PET-scans presented as the means of the % ID/g in the arthritic-, and healthy-ankles on day 1 (GPI n=3, control n=2), day 3 (GPI n=2, control n=2) and day 6 (GPI n=8, control n=4) after serum-transfer (left bars). We correlated ankle-swelling (mm) with the % ID/g values from the arthritic-ankles on days 1, 3 and 6 after serum-transfer (right). Mean values ± SD; $p<0.05$.

Figure 3

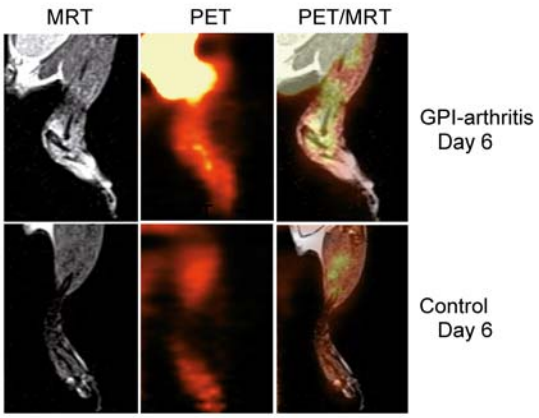

Localization of the exact ^{18}F-FMISO-uptake sites in arthritic- and control-ankles, using PET/MRI. A representative healthy-mouse after control-serum-injection exhibited no signs of hypoxia.

Figure 4

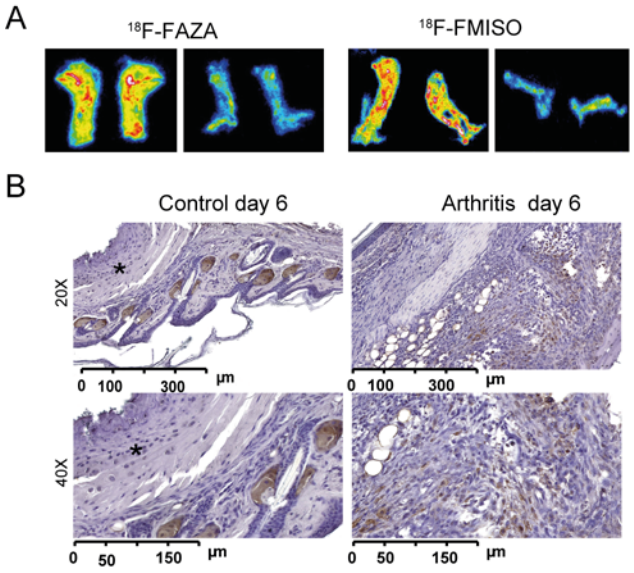

(A) Representative ^{18}F-FAZA–autoradiography analysis of slices from arthritic ankles on day 6 after GPI-serum transfer (left) and healthy ankles after control-serum application (right) confirming the *in vivo* ^{18}F-FAZA-PET-results. (B) Pimonidazole-immunohistochemistry from arthritic ankles 6 days after GPI-serum-transfer indicating areas of enhanced hypoxia compared with the healthy ankles.

Figure 5

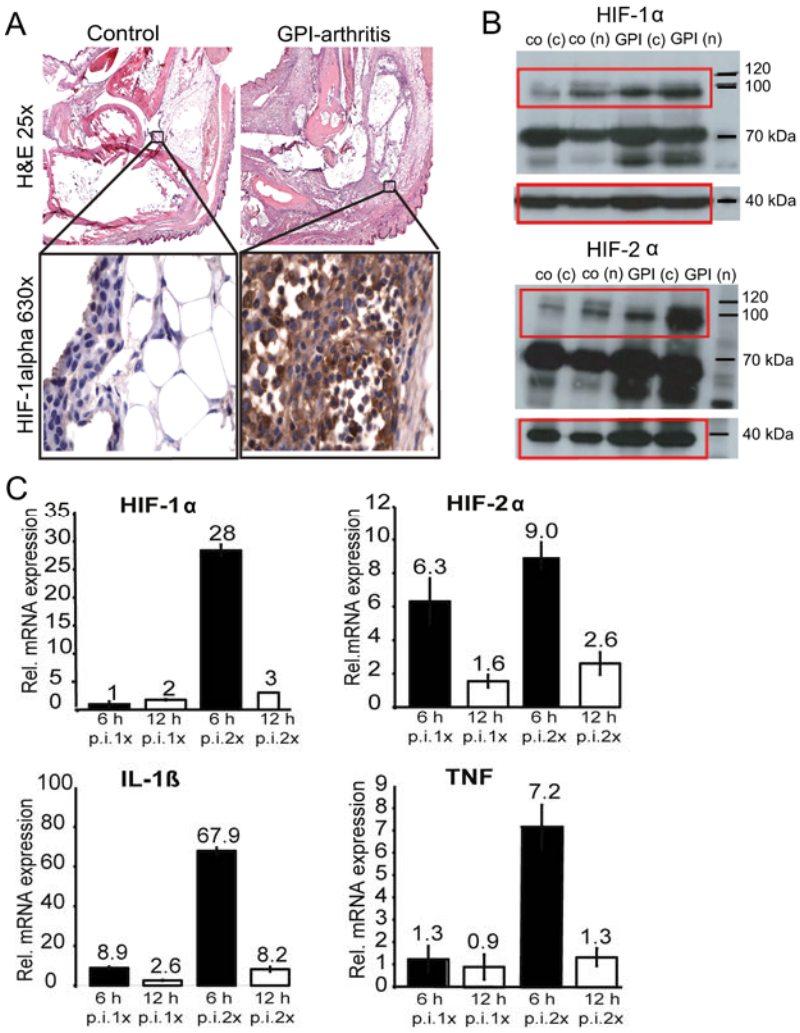

(A, upper images) Representative hematoxylin & eosin stained slides from GPI-arthritic ankles (n=2) on day 6 after GPI-serum transfer are shown. (A, lower images) HIF-1α (630x) staining (n=2) demonstrated an increased number of hypoxic cells comprised predominantly of neutrophils and synoviocytes. Control-ankles (n=2) exhibited no positive staining.

(B) HIF-1α and HIF-2α WB-analyses of arthritic-, (n=2) and healthy-ankles (n=2) 6 days after GPI- or control-serum transfer revealed strongly enhanced HIF-1α and HIF-2α protein-expressions. A control β-actin-staining was performed as indicated at 40 kDa. c=cytosolic fraction; n=nuclear fraction.

(C) RT-PCR was performed with ankle tissue from the mice 6-hours and 12-hours after a single GPI- or control-serum injection and with mouse ankle tissue from day 2 after the first and 6-hours and 12-hours after a second GPI- or control-serum injection. We detected the highest relative expressions of HIF-1α, HIF-2α, IL-1β and TNF, 6-hours after the second GPI-serum transfer; p.i.=post injection, h=hours.

Figure 6

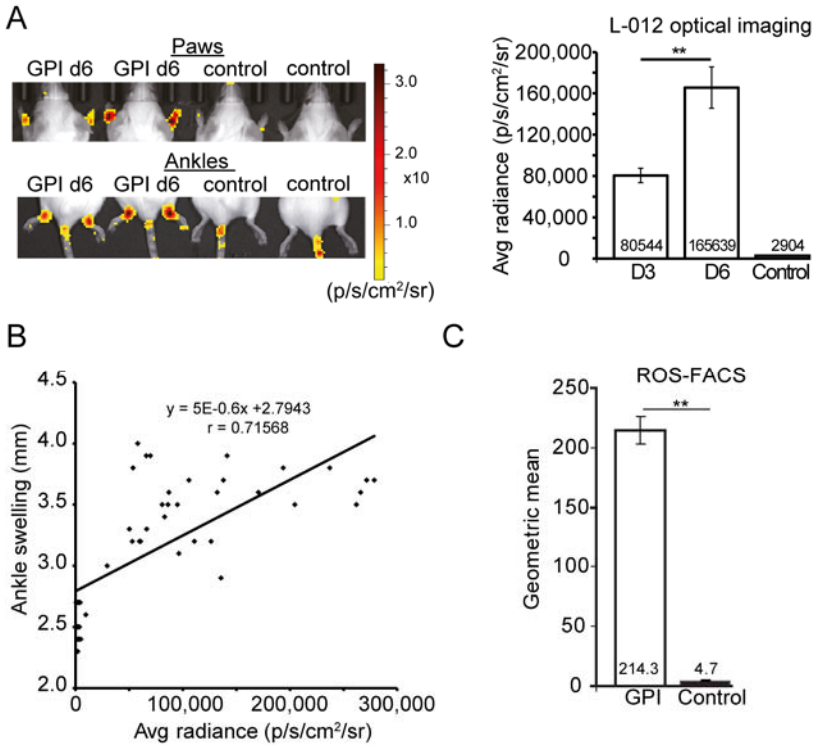

(A) L-012 chemiluminescence-imaging in mice after GPI- or control-serum injection using OI. Arthritic ankles exhibited high levels of L-012 expression compared with the control ankles (left panel). Quantitative analysis confirmed a significantly greater L-012 signals on days 3 (80544 p/s/cm^2/sr, n=8) and 6 (165639 p/s/cm^2/sr, n=8) after GPI-serum injection in the arthritic-, compared to healthy-ankles (2904 p/s/cm^2/sr) (n=9) (right panel). (B) We correlated ankle swelling [mm] with the Avg. Radiance [p/s/cm^2/sr] of L-012 in the arthritic-, and healthy-ankles at days 3 and 6 after GPI- or control-serum injection. (C) DHR-FACS analyses of the cells gained from the lavage of the arthritic-, and healthy-ankles revealed significantly greater ROS-levels in the arthritic-ankles than the controls. Mean values ± SD; $p<0.0001$

SUPPLEMENTAL MATERIAL & METHODS

GPI-Induced Arthritis

Blood sera containing monoclonal antibodies against GPI were obtained from the F1 generation of NOD/ShiltJ x K/B mice (K/BxN). Control sera were obtained from C57BL/6 mice. The sera were pooled and diluted 1:1 (volume/volume) with saline (200 µL), and the control- or GPI-serum was injected once intraperitoneal into female BALB/c mice between 7–12 weeks of age (Charles River, Sulzbach, Germany). For rtPCR, mice were injected with GPI- or control-serum on day 0 and a second time on day 2. Ankle thickness was determined with an Oditest micrometer (Kroeplin, Schlüchtern, Germany) before and at the indicated days after control or GPI serum transfer.

Fluorescence-Activated-Cell-Sorting Analysis

Cells from lavages of the arthritic- and healthy-ankles were evaluated using a dihydrorhodamine 123 flow-cytometry assay as described elsewhere (*1*) to determine the reactive oxygen intermediates in the arthritic-, (n=4) and healthy-ankles (n=4) at day 6 after GPI-, or control-serum injection.

Radiopharmaceuticals

^{18}F-FAZA and ^{18}F-FMISO were synthesized as previously described (*2*,*3*). In both cases the synthesizer TRACERlab FXF-N (GE Healthcare, Münster, Germany) was utilized. Radiochemical purity was always > 95% and molar activity > 50 GBq/µmol."

Autoradiography

For digital phosphor storage autoradiography-analysis, ^{18}F-FAZA-injected animals were sacrificed after the static PET-scans, and the ankles were obtained and cut into 20-µm slices at -20°C. Autoradiography was performed with a Storage Phosphor Screen (Molecular Dynamics, Sunnyvale, CA, USA). The phosphor-screen was scanned at a resolution of 50 µm/pixel with a STORM Phosphor-Imager (Molecular Dynamics) after an exposure-time of 24 h.

Simultaneous PET/MRI

PET/MRI was performed simultaneously using a custom built PET-insert that was placed into a 7-T small-animal MRI (ClinScan; Bruker Biospin MRI GmbH). The PET-insert was developed and built up in our laboratory. The measuring and reconstruction were performed as described elsewhere (*4*).

Histological Analyses

We performed H&E-staining and HIF-1α-immunohistochemistry to analyze the correlations with our *in vivo* data. H&E-, and immunohistochemical HIF-1α-staining (GPI n=2, control n=2) were performed according to standard procedures (5). Standardized procedures for HIF-1α-immunohistochemistry were performed using an automated immunostainer (Ventana Medical Systems, Inc., Tucson, AZ, USA) following the manufacturer´s protocols for open procedures with slight modifications. Appropriate positive- and negative-controls were used to confirm the adequacy of the staining.

To evaluate hypoxia *ex vivo*, pimonidazole (60 mg/kg, Hypoxyprobe Inc., Burlington, MA, USA) was injected *i.p.* into mice on day 6 after GPI-, (n=3) or control-serum (n=2), 50 min before the mice were sacrificed. The slides were analyzed using the HypoxyprobeTM-1 Plus Kit (Hypoxyprobe) with a FITC-conjugated mouse monoclonal primary antibody. We used an isotype antibody as a negative control. The images were scanned with a digital-slide-scanner (NanoZoomer 2.0-HT C9600, Hamamatsu Photonics, Ammersee, Germany).

Western Blot Analysis

The ankles of the arthritic-, and healthy-mice were freshly isolated, the tissue probes were homogenized and proteins were collected using the Nuclear Extract Kit (Active Motif, La Hulpe, Belgium). Aliquots of tissue lysate were separated on 8 % SDS-PAGE gels and transferred to Amersham HybondTM-P PVDF Transfer Membranes (GE Healthcare, Buckinghamshire, UK). The blots were probed with antibodies against HIF-1α or HIF-2α (GeneTex, CA, USA) overnight at 4 °C. The membranes were incubated using LumiGlo(R) Reagent and peroxide (Cell Signaling, MA, USA) and exposed to X-ray films (Amersham HyperfilmTM ECL, GE Healthcare Limited, UK). The membranes were re-probed for β-actin as a loading control.

Real-time Polymerase Chain Reaction (rtPCR)

Ankle tissues were homogenized in lysis buffer (peqGOLD Total RNA Kit, Peqlab, Erlangen, Germany), 6 h and 12 h after a single (day 0), and a second GPI- or control-serum injection (day 2). 2µg of RNA was subsequently transcribed using Superscript II Reverse Transcriptase (Invitrogen, Darmstadt, Germany). For the relative quantification by rtPCR in a LightCycler Real Time PCR System (Roche Diagnostics), 20 ng of cDNA was used. The relative mRNA expression levels of HIF-1α, HIF-2α, IL-1β and TNF were normalized against the housekeeping

gene aldolase. Used primers: aldolase (241bp), 5'-TGGGCCTTGACTTTCTCCTAT and 3'-TGTTGATGGAGCAGCCT-TAGT; HIF-1α (255bp): 5'-GATGCAGCAAGATCTCGGCGAAGC and 3'-GTCGCCGTCATCTGTTAGCACCATC; HIF-2α (230bp), 5'-AGTAGCCTCTGTGGCTCCAA and 3'-TCCAGGGCATGGTAGAACTC; IL-1β (313bp): 5'- TTTGACCTGGGCTGTCCTGATG and 3'-CATATGGGTCCGACAGCACGAG; TNF (212bp): 5'- AGCCCCCAGTCTGTATCCTT and 3'-CTCCCTTTGCAGAACTCAGG.

Statistical Data Analysis

The results were calculated as the means ± the standard deviations (SDs) if not stated otherwise. We used two-sample Student's t-tests to compare the ^{18}F-FMISO- and ^{18}F-FAZA-uptakes (% ID/g) in the joints using the JMP statistical software program (SAS Institute Inc., Cary, NC, USA; version 9). *P*-values <0.05 were regarded as statistically significant.

SUPPLEMENTAL DISCUSSION

Prolyl hydroxylase domain enzymes (PHDs) hydroxylate HIF-α subunits under normoxia, whereas under hypoxia PHDs lose their function leading to a HIF-α accumulation and translocation into the nucleus. The wide variety of PHD functions can be dependent or independent of HIF. PHDs sense not only oxygen but also various metabolites to obtain bioenergetic balance and organismal homeostasis. ROS have shown to be involved in the inhibition of PHDs activity due to its oxidization of ferrous iron to ferric iron (*6*).

Inflammation is frequently associated with ROS/ROS-stress that can catalyze or even protect against inflammatory disease progression. In addition to other cellular sources, ROS are generated in neutrophils that release myeloperoxidase and in macrophages that release the multi-enzyme complex nicotinamide adenine dinucleotide phosphate oxidase and myeloperoxidase (*7-9*). The cellular sources of ROS, i.e., neutrophils and macrophages, are both critically involved in experimental GPI-arthritis (*10,11*). ROS are classically defined as partially reduced metabolites of oxygen that possess strong oxidizing capabilities. At ‘‘physiological concentrations,’’ ROS act as mediators of inflammation and as signaling molecules that regulate cell growth, cell adhesion and differentiation, senescence, and apoptosis (*7-9*). Myeloperoxidase catalyzes the formation of hypochlorous-acid which is a powerful oxidant derived from chloride-ions and hydrogen-peroxide. ROS are rapidly diffusing short-lived messenger molecules that are generated as bystander products of cellular metabolism through the electron transport chain in the mitochondria as well as via cytochrome P450. ROS, such as superoxide anions, can rapidly combine with NO to form RNS, such as peroxynitrite, which adds to the pro-inflammatory burden of ROS (*7,9*). Various enzymes can generate cellular ROS, including xanthine oxidases, cyclooxygenases, NO synthases, mitochondrial oxidases, and the nicotinamide adenine dinucleotide phosphate oxidases. A major ROS-source is the nicotinamide-adenine-dinucleotide-phosphate-oxidases (mainly expressed by phagocytes and endothelial cells) (*7,9,12*).

Furthermore, oxidation by ROS can lead to the activation of inactive proteases (*13*). Antioxidants can prevent this process (*14*). We recently have shown that the ROS-scavenger N-acetylcysteine suppresses the inflammatory immune-response and the *in vivo* activation of matrix-metalloprotease (MMP) in an experimental model of contact-hypersensitivity-reaction. In this study we determined MMP-activity with OI using a specifically activatable-probe (*15*). Activatable-probes are designed to be optically silent in its inactivated state due to the quenching of the signal by Förster resonance energy transfer. After cleaving of the specific peptide sequence by activated specific proteases,

such as MMPs, a fluorescence-signal can be detected *in vivo* by OI (*16*). MMP-activation is critically involved in the establishment of RA (*17*).

SUPPLEMENTAL FIGURES

Supplemental Figure 1

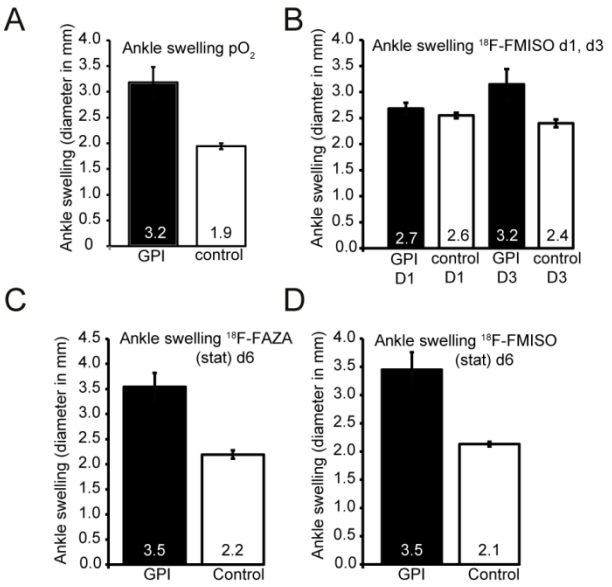

Ankle swelling (diameter in mm) in the experimental mice measured with a pO_2-probe (A) on day 6 after GPI- or control-serum injection. (B) Ankle thickening in the GPI- and control-serum injected mice investigated on days 1, 3 and 6 (D) by ^{18}F-FMISO-PET. (C) Ankle thickening in GPI- and control-serum injected mice investigated with ^{18}F-FAZA-PET on day 6 after serum transfer.

Supplemental Figure 2

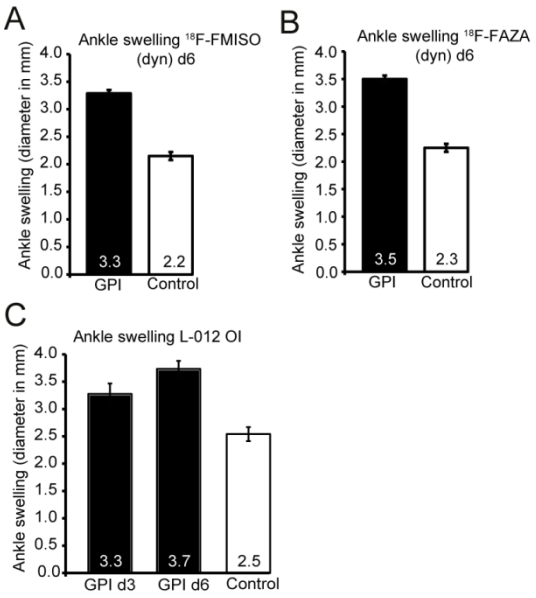

Ankle swelling (diameter in mm) in the experimental mice on day 6 after GPI- or control-serum injection measured dynamically with ^{18}F-FMISO (A) and ^{18}F-FAZA on day 6 (B). Ankle thickening in GPI- and control-serum injected mice investigated on days 3 and 6 using L-012-OI to measure ROS *in vivo* (C).

SUPPLEMENTAL REFERENCES

1. Richardson MP, Ayliffe MJ, Helbert M, Davies EG. A simple flow cytometry assay using dihydrorhodamine for the measurement of the neutrophil respiratory burst in whole blood: comparison with the quantitative nitrobluetetrazolium test. *J Immunol Methods.* 1998;219:187-193.

2. Reischl G, Ehrlichmann W, Bieg C, et al. Preparation of the hypoxia imaging PET tracer [18F]FAZA: reaction parameters and automation. *Appl Radiat Isot.* 2005;62:897-901.

3. Patt M, Kuntzsch M, Machulla HJ. Preparation of [F-18]fluoromisonidazole by nucleophilic substitution on THP-protected precursor: yield dependence on reaction parameters. *J Radioanal Nucl Chem.* 1999;240:925-927.

4. Wehrl HF, Hossain M, Lankes K, et al. Simultaneous PET-MRI reveals brain function in activated and resting state on metabolic, hemodynamic and multiple temporal scales. *Nat Med.* 2013;19:1184-1189.

5. Kneilling M, Hultner L, Pichler BJ, et al. Targeted mast cell silencing protects against joint destruction and angiogenesis in experimental arthritis in mice. *Arthritis Rheum.* 2007;56:1806-1816.

6. Wong BW, Kuchnio A, Bruning U, Carmeliet P. Emerging novel functions of the oxygen-sensing prolyl hydroxylase domain enzymes. *Trends Biochem Sci.* 2013;38:3-11.

7. Forman HJ, Torres M. Redox signaling in macrophages. *Mol Aspects Med.* 2001;22:189-216.

8. Hultqvist M, Olsson LM, Gelderman KA, Holmdahl R. The protective role of ROS in autoimmune disease. *Trends Immunol.* 2009;30:201-208.

9. De Ravin SS, Naumann N, Cowen EW, et al. Chronic granulomatous disease as a risk factor for autoimmune disease. *J Allergy Clin Immunol.* 2008;122:1097-1103.

10. Solomon S, Rajasekaran N, Jeisy-Walder E, Snapper SB, Illges H. A crucial role for macrophages in the pathology of K/B x N serum-induced arthritis. *Eur J Immunol.* 2005;35:3064-3073.

11. Wipke BT, Allen PM. Essential role of neutrophils in the initiation and progression of a murine model of rheumatoid arthritis. *J Immunol.* 2001;167:1601-1608.

12. Dragin N, Smani M, Arnaud-Dabernat S, et al. Acute oxidative stress is associated with cell proliferation in the mouse liver. *FEBS Lett.* 2006;580:3845-3852.

13. Kessenbrock K, Plaks V, Werb Z. Matrix metalloproteinases: regulators of the tumor microenvironment. *Cell.* 2010;141:52-67.

14. Cook-Mills JM. Hydrogen peroxide activation of endothelial cell-associated MMPs during VCAM-1-dependent leukocyte migration. *Cell Mol Biol (Noisy-le-grand).* 2006;52:8-16.

15. Schwenck J, Griessinger CM, Fuchs K, et al. In vivo optical imaging of matrix metalloproteinase activity detects acute and chronic contact hypersensitivity reactions and enables monitoring of the antiinflammatory effects of N-acetylcysteine. *Mol Imaging.* 2014;13.

16. Bremer C, Tung CH, Weissleder R. In vivo molecular target assessment of matrix metalloproteinase inhibition. *Nat Med.* 2001;7:743-748.

17. Ibarra JM, Jimenez F, Martinez HG, Clark K, Ahuja SS. MMP-activated fluorescence imaging detects early joint inflammation in collagen-antibody-induced arthritis in cc-chemokine receptor-2-null mice, in-vivo. *Int J Inflam.* 2011;2011:691587.